Phenomenological model of the third-harmonic magnetic response due to superconducting fluctuations: Application to Sr2RuO4

Chen, Fei; Pelc, Damjan; Greven, Martin; Fernandes, Rafael M.

Download date / Datum preuzimanja: **2025-03-29**

Phenomenological model of the third-harmonic magnetic response due to superconducting fluctuations: Application to Sr₂RuO₄

Fei Chen [●],[1] Damjan Pelc,[1,2] Martin Greven,[1] and Rafael M. Fernandes[1]

[1]*School of Physics and Astronomy, University of Minnesota, Minneapolis, Minnesota 55455, USA*
[2]*Department of Physics, Faculty of Science, University of Zagreb, Bijenička 32, HR-10000 Zagreb, Croatia*

We employ the phenomenological Lawrence-Doniach model to compute the contributions of the superconducting fluctuations to the third-harmonic magnetic response, denoted here by $\overline{M}_3$, which can be measured in a precise way using ac magnetic fields and lock-in techniques. We show that, in an intermediate temperature regime, this quantity behaves as the third-order nonlinear susceptibility, which shows a power-law dependence with the reduced temperature $\epsilon = \frac{T - T_c}{T_c}$ as $\epsilon^{-5/2}$. Very close to T_c, however, $\overline{M}_3$ saturates due to the nonzero amplitude of the ac field. We compare our theoretical results with experimental data for three conventional superconductors—lead, niobium, and vanadium—and for the unconventional superconductor Sr₂RuO₄ (SRO). We find good agreement between theory and experiment for the elemental superconductors, although the theoretical values for the critical field systematically deviate from the experimental ones. In the case of SRO, however, the phenomenological model completely fails to describe the data, as the third-harmonic response remains sizable over a much wider reduced temperature range compared to Pb, Nb, and V. We show that an inhomogeneous distribution of T_c across the sample can partially account for this discrepancy, since regions with a locally higher T_c contribute to the fluctuation $\overline{M}_3$ significantly more than regions with the "nominal" T_c of the clean system. However, the exponential temperature dependence of $\overline{M}_3$ first reported by Pelc *et al.* [Nat. Commun. **10**, 2729 (2019)] is not captured by the model with inhomogeneity. We conclude that, while inhomogeneity is an important ingredient to understand the superconducting fluctuations of SRO and other perovskite superconductors, additional effects may be at play, such as non-Gaussian fluctuations or rare-region effects.

I. INTRODUCTION

In unconventional superconductors, not only the gap function but also the superconducting fluctuations can be quite different from their conventional counterparts (for reviews, see Refs. [1–3]). Indeed, several high-T_c superconductors have strongly anisotropic properties and small coherence lengths, suggestive of a wider temperature range in which fluctuations are important. Moreover, the magnitude of these fluctuations as well as their temperature dependence can also display unusual behaviors [4]. Signatures of superconducting fluctuations have been widely probed in both conventional and unconventional superconductors, in observables as diverse as specific heat [5–7], linear and nonlinear conductivity [8–15], microwave and terahertz response [15–19], susceptibility [20–25], and the Nernst coefficient [26–30].

Experimentally, one of the main difficulties is to unambiguously identify contributions that can be uniquely attributed to superconducting fluctuations, since these are usually small compared to the regular normal-state contributions [20]. Theoretically, modeling contributions of superconducting fluctuations to the magnetic susceptibility and to the conductivity, both phenomenologically and microscopically, dates back several decades [31–39]. More recent studies on superconducting fluctuations have focused on the role of phase fluctuations [40], on disordered two-dimensional (2D) superconductors [41], and on thermal and electric transport properties above T_c in cuprates [42–48].

Recently, a method to probe superconducting fluctuations based on the third-harmonic magnetic response was put forward in Ref. [4]. Specifically, an ac magnetic field $H(t) = H_0 \cos(\omega t)$ is applied and the magnetization is measured at a frequency 3ω. This observable, which we hereafter denote by $\overline{M}_3$, is related to, but not identical to, the standard nonlinear susceptibility χ_3. The key point is that the third-harmonic response $\overline{M}_3$ is vanishingly small in the normal state. This is indeed reflected in the data for the conventional superconductors reported in this work: in all cases studied here, the signal decreases sharply above T_c, and becomes essentially undetectable in the normal state. In contrast, the linear susceptibility is known to remain sizable well above T_c. As a result, its magnitude and temperature dependence near the superconducting transition temperature T_c should be dominated by superconducting fluctuations. In Ref. [4], it was empirically found that $\overline{M}_3$ displays an unusual exponential temperature dependence in perovskite-based superconductors such as cuprates, Sr₂RuO₄ (SRO), and SrTiO₃, as opposed to a power-law temperature dependence in standard electron-phonon superconductors. However, the implications

of these observations for the nature of superconducting fluctuations in unconventional superconductors remain unsettled.

In this paper, we employ a phenomenological approach based on the Lawrence-Doniach (LD) [49] free energy to compute the contributions to the experimentally measured quantity $\overline{M}_3$ of Ref. [4] arising from Gaussian superconducting fluctuations. The main appeal of such an approach is that, being phenomenological, it is potentially applicable to both conventional and unconventional superconductors. In particular, we perform a quantitative comparison between the theoretical results predicted by the LD formalism and the data on several elemental superconductors (Pb, Nb, and V) and on the unconventional superconductor SRO. We find that the LD result provides a good description of the data for elemental superconductors over a wide range of reduced temperature values, $\epsilon \equiv \frac{T-T_c}{T_c}$, and correctly captures the observed 5/2 power-law behavior of $\overline{M}_3$ for intermediate values of ϵ. The theoretically extracted values for the zero-temperature upper critical field $H_{c2}(0)$ differ by factors of 2 to 6 from the experimental ones; we argue that this difference could be an artifact of the LD model, which was developed for layered superconductors rather than cubic systems. Overall, the results demonstrate that measurements of the third-harmonic magnetic response are indeed a powerful probe of superconducting fluctuations.

However, in the case of Sr$_2$RuO$_4$, we find a sharp disagreement between the LD theoretical results and the data for $\overline{M}_3$. Both the temperature dependence and the magnitude of $\overline{M}_3$ near T_c are not captured by the theoretical model. Motivated by the evidence for significant inhomogeneity in several perovskite-based superconductors [4,15,50], we modify our LD model for $\overline{M}_3$ and include a distribution of T_c values. We find that even a modest width of this T_c distribution is capable of capturing the typical values of $\overline{M}_3$ observed experimentally. However, this modification is not sufficient to explain the exponential temperature dependence reported in Ref. [4]. We thus conclude that while inhomogeneity at the mean-field level is important to elucidate the behavior of superconducting fluctuations in Sr$_2$RuO$_4$, it is likely not the sole reason for the observed exponential temperature dependence. One possibility is that such behavior arises from rare-region contributions [4,50,51] (i.e., large-volume regions of the sample devoid of defects, which have an exponentially small probability of emerging in a randomly disordered system) or from non-Gaussian fluctuations, which are absent in the LD model employed here.

The paper is organized as follows: In Sec. II, we employ the LD model to derive an expression for the third-harmonic magnetic response $\overline{M}_3$, and discuss the temperature dependence of this quantity in different regimes. Section III presents a quantitative comparison between the theoretical and experimental results for three conventional superconductors (Pb, Nb, and V) and the unconventional superconductor Sr$_2$RuO$_4$. We note that some of the data were previously published in Ref. [4]. An extension of the model presented in Sec. II that includes the role of inhomogeneity is also introduced. Our conclusions are presented in Sec. IV.

II. PHENOMENOLOGICAL MODEL FOR THE THIRD-HARMONIC MAGNETIC RESPONSE

In this section, we derive an expression for the third-harmonic magnetic response $\overline{M}_3$, measured in the experiments of Ref. [4], based on the LD approach. We first review the contribution of the superconducting fluctuations to the magnetization in the presence of a static magnetic field within the LD approach. Here we only quote the LD results, which are well known from the literature (for their derivations, see, for instance, Refs. [2,52]). Using the LD results, we then proceed to include an ac field to explicitly calculate $\overline{M}_3$, and discuss its temperature dependence in different regimes.

A. Linear and nonlinear susceptibilities in the Lawrence-Doniach model

Fluctuations of a superconductor in the presence of an external magnetic field can be modeled within the phenomenological Ginzburg-Landau framework. In a regime close to T_c, the general superconducting Ginzburg-Landau free-energy functional takes the form

$$\Delta \mathcal{F}[\Psi(\mathbf{x})] = \int d^d x \bigg(a|\Psi|^2 + \frac{b}{2}|\Psi|^4 + \frac{1}{4m}\bigg|\bigg(\frac{\boldsymbol{\nabla}}{i} - 2e\mathbf{A}\bigg)\Psi\bigg|^2 + \frac{1}{8\pi}|\boldsymbol{\nabla} \times \mathbf{A}|^2 \bigg). \quad (1)$$

Here, $\Psi(\mathbf{x})$ is the superconducting order parameter, $2m$ and $2e$ are the effective mass and charge of a Cooper pair, $\mathbf{A}$ is the vector potential, and $b > 0$ is a Ginzburg-Landau parameter. The coefficient a is parametrized as $a = \alpha(T - T_c) = \alpha T_c \epsilon$, where $\epsilon = \frac{T-T_c}{T_c}$ is the reduced temperature and α a positive constant. Near T_c, but above the temperature range where critical fluctuations become important, as set by the Ginzburg-Levanyuk parameter, one assumes that the order parameter is small and slowly varying. As a result, the quartic term in Eq. (1) can be neglected, and only Gaussian fluctuations are considered:

$$\Delta \mathcal{F}[\Psi(\mathbf{x})] = \int d^d x \bigg(a|\Psi|^2 + \frac{1}{4m}\bigg|\bigg(\frac{\boldsymbol{\nabla}}{i} - 2e\mathbf{A}\bigg)\Psi\bigg|^2 \bigg). \quad (2)$$

To obtain the LD free-energy expression, one assumes a layered superconductor and considers a magnetic field H applied perpendicular to the layers. A detailed derivation can be found in standard textbooks and review papers (see, for instance, Refs. [2,52]). For completeness, we only highlight the main steps of the derivation and quote the results from Ref. [2]. Because of the layered nature of the system, there is a difference between in-plane and out-of-plane kinetic terms. While the former assumes the same form as in Eq. (1), the latter is described by $\delta_z|\Psi_{l+1} - \Psi_l|^2$, where δ_z is the interlayer coupling constant and the subscript l is a layer index. It is also convenient to introduce two dimensionless quantities, h and r. By using the result $H_{c2}(0) = \frac{2m\alpha T_c}{e}$ for the zero-temperature critical field, we define the dimensionless applied field $h \equiv \frac{H}{H_{c2}(0)}$. Moreover, we define the dimensionless anisotropy parameter $r \equiv \frac{2\delta_z}{\alpha T_c}$, which can also be expressed in terms of the ratio between the correlation length along the z direction,
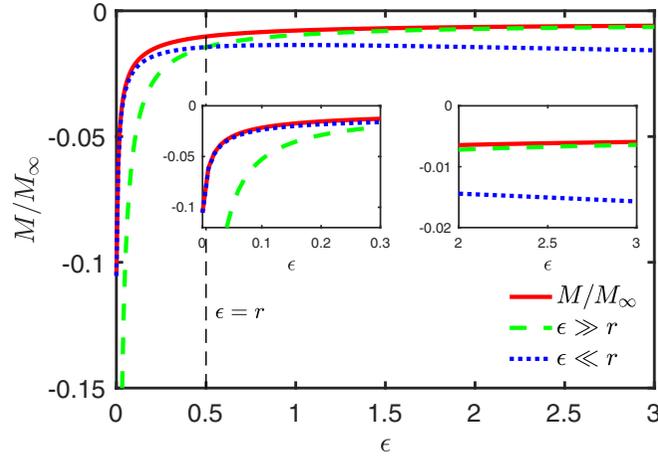
FIG. 1. Magnetization (red curve, in units of M_∞) induced by superconducting fluctuations, in the presence of a dc field h, as a function of the reduced temperature ϵ according to Eq. (4). We also include for comparison the asymptotic expressions for $M(\epsilon \gg r)$ (green dashed curve) and $M(\epsilon \ll r)$ (blue dotted curve), Eqs. (6) and (7), respectively. A crossover clearly takes place when $\epsilon \sim r$. The dimensionless parameters chosen here were $h = 0.01$, $r = 0.5$. The insets are zooms on different temperature ranges.

$\xi_z(0)$, and the interlayer separation s, $r = \frac{4\xi_z^2(0)}{s^2}$. Writing the order parameter in a product form between in-plane Landau-level wave functions and plane waves propagating along the z direction, one can evaluate the partition function $Z = \int D\Psi D\Psi^* e^{-\frac{\Delta \mathcal{F}[\Psi(\mathbf{x})]}{T}}$ and then obtain the LD free-energy expression (up to a constant) [2,52]:

$$\frac{F(\epsilon)}{M_\infty H_{c2}(0)} = -\frac{2(\epsilon+1)h}{\ln 2}\left[\left(\epsilon + \frac{r}{2}\right)\frac{\ln h}{2h} - \frac{1}{2}\ln 2\pi + \int_0^{\pi/2}\frac{d\phi}{\pi/2}\ln \Gamma\left(\frac{1}{2} + \frac{\epsilon + r\sin^2\phi}{2h}\right)\right]. \tag{3}$$

Here, $\Gamma(x)$ is the gamma function, the integration over the variable ϕ effectively sums over the layers, v is the volume, and $M_\infty \equiv \frac{T_c}{\Phi_0 s}\frac{\ln 2}{2}$ is the absolute value of the saturation magnetization at T_c, with Φ_0 denoting the flux quantum. Similarly, the LD expression for the magnetization is given by [2,52]

$$\frac{M(\epsilon)}{M_\infty} = -\frac{2(\epsilon+1)}{\ln 2}\int_0^{\pi/2}\frac{d\phi}{\pi/2}\left\{\frac{\epsilon + r\sin^2\phi}{2h}\left[\psi\left(\frac{\epsilon + r\sin^2\phi}{2h} + \frac{1}{2}\right) - 1\right] - \ln \Gamma\left(\frac{\epsilon + r\sin^2\phi}{2h} + \frac{1}{2}\right) + \frac{1}{2}\ln 2\pi\right\}, \tag{4}$$

where $\psi(x) = \frac{d\ln\Gamma(x)}{dx}$ is the digamma function. By taking $h \gg \epsilon$, r in Eq. (4), the right-hand side gives -1 at $\epsilon = 0$, confirming that M_∞ is the saturation magnetization at T_c. Note that this expression is valid for $h > 0$; in the case of $h < 0$, symmetry implies $F(-h) = F(h)$ and $M(-h) = -M(h)$. For future reference, we list the three dimensionless parameters that will be employed throughout this work:

$$\epsilon = \frac{T - T_c}{T_c}, \quad r = \left[\frac{2\xi_z(0)}{s}\right]^2, \quad h = \frac{H}{H_{c2}(0)}. \tag{5}$$

While the anisotropy parameter r is fixed, its impact on the magnetization depends on the temperature range probed. In a regime sufficiently far from T_c, $r \ll \epsilon$, the system essentially behaves as decoupled layers ($r \to 0$) and Eq. (4) becomes [2,52]

$$\frac{M(\epsilon \gg r)}{M_\infty} = -\frac{2(\epsilon+1)}{\ln 2}\left\{\frac{\epsilon}{2h}\left[\psi\left(\frac{1}{2} + \frac{\epsilon}{2h}\right) - 1\right] - \ln\frac{\Gamma\left(\frac{1}{2} + \frac{\epsilon}{2h}\right)}{\sqrt{2\pi}}\right\}. \tag{6}$$

On the other hand, as T_c is approached, the system will eventually cross over to the regime $r \gg \epsilon$. Then, the three-dimensional nature of the system cannot be neglected, and the magnetization becomes [2,38,52]

$$\frac{M(\epsilon \ll r)}{M_\infty} = -\frac{6(\epsilon+1)}{\ln 2}\left(\frac{2}{r}\right)^{1/2}\sqrt{h}\left[\zeta\left(-\frac{1}{2}, \frac{1}{2} + \frac{\epsilon}{2h}\right) - \frac{1}{3}\zeta\left(\frac{1}{2}, \frac{1}{2} + \frac{\epsilon}{2h}\right)\frac{\epsilon}{2h}\right], \tag{7}$$

where $\zeta(v, x)$ is the Hurwitz zeta function.

Therefore, as T_c is approached from above, we expect a crossover of the temperature-dependent magnetization from 2D-like behavior to three-dimensional (3D)-like behavior, with the crossover temperature corresponding to $\epsilon \sim r$. This general behavior is illustrated in Fig. 1, where M given by Eq. (4) is plotted as a function of the reduced temperature ϵ together with the asymptotic expressions in Eqs. (6) and (7) for a fixed field value. As expected, the contribution of the superconducting fluctuations to the magnetization is negative.

It will be useful later to contrast the temperature dependence of the third-harmonic response $\overline{M}_3$ with that of the nonlinear magnetic susceptibility. To derive the latter, we consider the limit of small fields, i.e., when the dimensionless magnetic field is the smallest parameter of the problem, $h \ll \epsilon, r$. Going back to the main expression for the magnetization in Eq. (4), it is convenient to define $y = \frac{\epsilon + r\sin^2\phi}{2h}$. Since $h \ll \epsilon, r$, it follows that $y \gg 1$ and the integrand can be expanded as

$$y\left[\psi\left(y + \frac{1}{2}\right) - 1\right] - \ln\Gamma\left(y + \frac{1}{2}\right) + \frac{1}{2}\ln(2\pi) = \frac{1}{12y} - \frac{7}{720y^3} + \frac{31}{6720y^5} + \mathcal{O}(x^{-7}). \tag{8}$$

The integrals over ϕ can be analytically evaluated. Expanding the magnetization in odd powers of h,

$$\frac{M}{M_\infty} = \chi_1 h + \chi_3 h^3 + \chi_5 h^5 + \mathcal{O}(h^7), \tag{9}$$

we find the following expressions for the linear and nonlinear susceptibilities (see also Refs. [52,53]):

$$\chi_1 = -\frac{(1+\epsilon)}{3\ln 2}\frac{1}{\epsilon^{1/2}\sqrt{\epsilon+r}}, \tag{10}$$

$$\chi_3 = \frac{7(1+\epsilon)}{360\ln 2}\frac{(3r^2 + 8r\epsilon + 8\epsilon^2)}{\epsilon^{5/2}(\epsilon+r)^{5/2}}, \tag{11}$$

$$\chi_5 = -\frac{31(1+\epsilon)}{13440\ln 2}\frac{(35r^4 + 160r^3\epsilon + 288r^2\epsilon^2 + 256r\epsilon^3 + 128\epsilon^4)}{\epsilon^{9/2}(\epsilon+r)^{9/2}}. \tag{12}$$

Close enough to T_c, when $\epsilon \ll r$, we find the following power-law behaviors:

$$\chi_1 \sim -\frac{\epsilon^{-1/2}}{\sqrt{r}}, \tag{13}$$

$$\chi_3 \sim \frac{\epsilon^{-5/2}}{\sqrt{r}}, \tag{14}$$

$$\chi_5 \sim -\frac{\epsilon^{-9/2}}{\sqrt{r}}. \tag{15}$$

B. The third-harmonic magnetic response $\overline{M}_3$: Experimental setup and theory

One of the most common experimental probes of superconducting fluctuations is to apply a dc magnetic field and measure the magnetic response [see Eq. (9)]. The key issue with measuring the linear susceptibility χ_1 is that the diamagnetic contribution due to the superconducting fluctuations is typically much smaller than the paramagnetic contributions from other normal-state degrees of freedom. For the nonlinear susceptibility χ_3, however, one generally expects that the intrinsic normal-state contribution is negligible in most cases, which could in principle allow one to assess the contribution from the superconducting fluctuations in a more unambiguous fashion. Note that, while in principle the susceptibilities χ_1 and χ_3 are tensor quantities, our experimental setup is designed in such a way that both the excitation and detection coils are along the same axis. We therefore only measure in-plane diagonal components, which are equivalent for a tetragonal or cubic system. Hereafter we refer only to a scalar χ_3.

Instead of applying a dc magnetic field, the experimental technique presented in Ref. [4] and utilized here employs an ac field (of the form $H_0\cos\omega t$) and a system of coils to measure the oscillating sample magnetization. In order to determine the third-order response, a lock-in amplifier is used at the third harmonic of the fundamental frequency ω, which is

typically in the kilohertz range. If the fifth-order susceptibility is significantly smaller than the third-order susceptibility, the third-harmonic response is a good measure of the third-order susceptibility. This condition was experimentally verified by measuring at the fifth harmonic, where the signal was found to be vanishingly small except for extremely close to T_c, where it was still an order of magnitude smaller than the third harmonic. We can thus safely ignore the higher-order contributions. Most of the data presented here were published in Ref. [4], and were obtained in two separate experimental setups. Low-temperature measurements on strontium ruthenate were performed in a ^{3}He evaporation refrigerator with a custom-made set of coils. Samples of conventional superconductors were measured in a modified Quantum Design magnetic property management system (MPMS), where we used the built-in ac susceptibility coil to generate the excitation magnetic field, and a custom-made probe with small detection coils to maximize the filling factor. We estimate that the magnetization sensitivity of both setups is better than 1 nanoemu, an improvement of one to two orders of magnitude over standard superconducting quantum interference device (SQUID)-based instruments. This is made possible by lock-in detection, matching the impedance of the detection coils and lock-in amplifier inputs, and large filling factors of the detection coils [54].

Although we expect the third-harmonic response to exhibit behavior similar to the third-order nonlinear susceptibility χ_3, there are important differences, since the amplitude of the oscillating field, albeit small ($H_0 \sim 1$ Oe), is nonzero. Thus, to provide a more direct comparison between the LD model and experiments, we directly compute the third-harmonic response, which we denote by $\overline{M}_3$. In our experimental setup, the signal corresponds to the Fourier transform of $\frac{\partial M}{\partial t}$ at 3ω,

$$\overline{M}_3(\epsilon) = \int_{-\frac{\pi}{\omega}}^{\frac{\pi}{\omega}} \frac{\partial M(\epsilon, h(t))}{\partial t} e^{3i\omega t}dt, \tag{16}$$
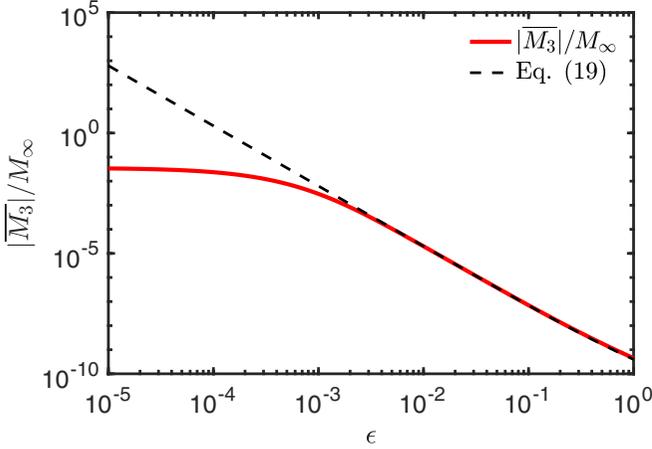
FIG. 2. Absolute value of the third-harmonic response, $|\overline{M}_3|$ in Eq. (17), in units of M_∞, as a function of the reduced temperature $\epsilon \equiv \frac{T - T_c}{T_c}$, plotted on a log-log scale (red curve). The dashed black line corresponds to the analytical approximation in Eq. (19), which gives an $\epsilon^{-5/2}$ power-law behavior. The dimensionless parameters used here are $h_0 = 10^{-3}$ and $r = 1$.

where $M(\epsilon, h(t))$ is obtained from Eq. (4) by substituting $h = h_0 \cos \omega t$. Integration by parts gives $\overline{M}_3(\epsilon) = -3i \int_{-\pi}^{\pi} M(\epsilon, h_0 \cos \theta) e^{3i\theta} d\theta$ with $\theta = \omega t$. Using the fact that $M(\epsilon, -h) = -M(\epsilon, h)$, we have $\int_{-\pi}^{-\pi/2} M(\epsilon, h_0 \cos \theta) e^{i3\theta} d\theta = \int_0^{\pi/2} M(\epsilon, h_0 \cos \theta) e^{i3\theta} d\theta$ and $\int_{\pi/2}^{\pi} M(\epsilon, h_0 \cos \theta) e^{i3\theta} d\theta = \int_{-\pi/2}^{0} M(\epsilon, h_0 \cos \theta) e^{i3\theta} d\theta$, which yields

$$\overline{M}_3(\epsilon) = -6i \int_{-\pi/2}^{\pi/2} d\theta \, M(\epsilon, h_0 \cos \theta) \cos 3\theta, \qquad (17)$$

where the field $h_0 \cos \theta$ remains positive between the integration limits. Experimentally, both the imaginary and real parts can be measured. However, due to issues with lock-in phase determination in third-harmonic measurements [54], we simply use the absolute value of $\overline{M}_3$ for comparison between the experimental and theoretical results.

In the temperature range where $h_0 \ll \epsilon$, we can substitute the series expansion (9) in Eq. (17) and find

$$\frac{|\overline{M}_3|}{M_\infty} \approx \frac{3\pi}{4} \chi_3 h_0^3 + \frac{15\pi}{16} \chi_5 h_0^5. \qquad (18)$$

Now, in the relevant regime $r \gg \epsilon$, according to Eqs. (14), we have $\chi_3 \sim \epsilon^{-5/2}$ and $\chi_5 \sim \epsilon^{-9/2}$. Therefore, as long as we remain in the regime $h_0 \ll \epsilon$, the contribution from the fifth-order nonlinear susceptibility χ_5 can be neglected. Using Eq. (11) we obtain

$$\frac{|\overline{M}_3|}{M_\infty} \approx \left(\frac{7\pi}{160 \ln 2} \right) \frac{h_0^3 (1 + \epsilon) \epsilon^{-5/2}}{\sqrt{r}}. \qquad (19)$$

Therefore, we expect that, in the temperature range $h_0 \ll \epsilon \ll r$, the third-harmonic response $|\overline{M}_3|$ displays the power-law behavior $(T - T_c)^{-5/2}$ characteristic of the third-order nonlinear susceptibility χ_3. To verify this behavior explicitly, in Fig. 2 we present the numerically calculated $|\overline{M}_3|$ for $h_0 = 10^{-3}$ and $r = 1$, and compare it with the analytical approximation in Eq. (19). It is clear that the expected power-law
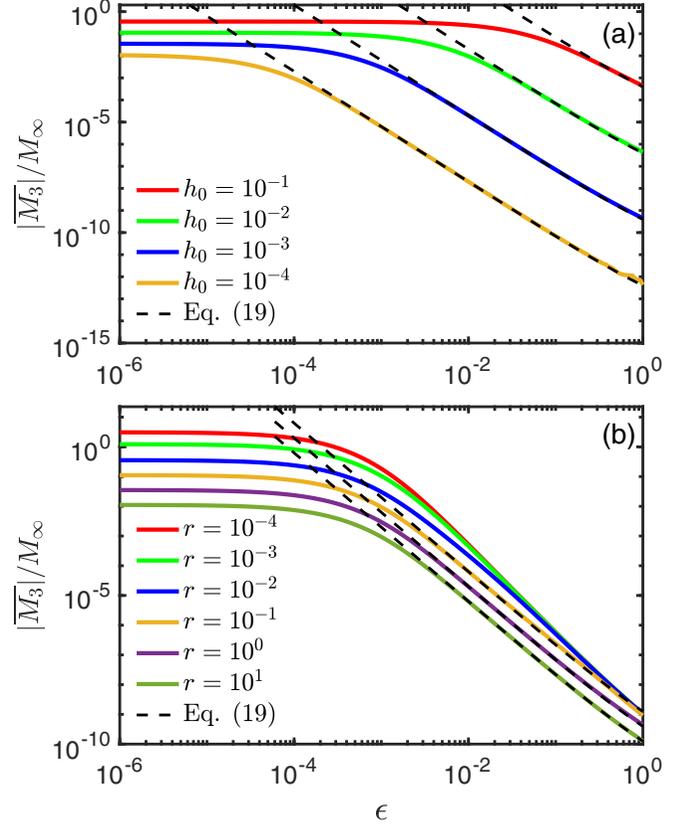

FIG. 3. Absolute value of the third-harmonic response $|\overline{M}_3|$ (in units of M_∞) as a function of the reduced temperature ϵ for (a) varying h_0 values (fixed $r = 1$) and (b) varying r values (fixed $h_0 = 10^{-3}$). The dashed lines mark the power-law behavior $\epsilon^{-5/2}$ displayed by the curves with larger values of r.

behavior appears over a rather wide temperature range. As one approaches T_c from above and reaches the temperature scale $\epsilon \sim h_0$, deviations from the power-law are observed, and $|\overline{M}_3|$ saturates to a constant value. This is a direct consequence of the fact that we are not computing the dc susceptibility, but the ac third-harmonic response at a fixed field amplitude h_0. Figures 3(a) and 3(b) depict how the temperature window in which power-law behavior is observed is affected by changing r and h_0. As expected, increasing h_0 significantly suppresses the window of power-law behavior, as the temperature scale $\epsilon \sim h_0$ is moved up. On the other hand, the anisotropy parameter r has a rather minor impact on the temperature range in which $\epsilon^{-5/2}$ behavior is observed.

III. COMPARISON WITH EXPERIMENTAL DATA

A. Conventional superconductors (Pb, Nb, and V)

In order to validate the LD approach for the third-harmonic response, we first compare the theoretical results for $\overline{M}_3$ from Eq. (17) with the experimental third-harmonic data for three conventional elemental superconductors: lead (Pb), niobium (Nb), and vanadium (V). Besides an overall prefactor, there are three fitting parameters in our formalism: the upper critical field H_{c2}, the critical temperature T_c, and the anisotropy ratio r. The field H_0 is 1.3 Oe as generated by the excitation
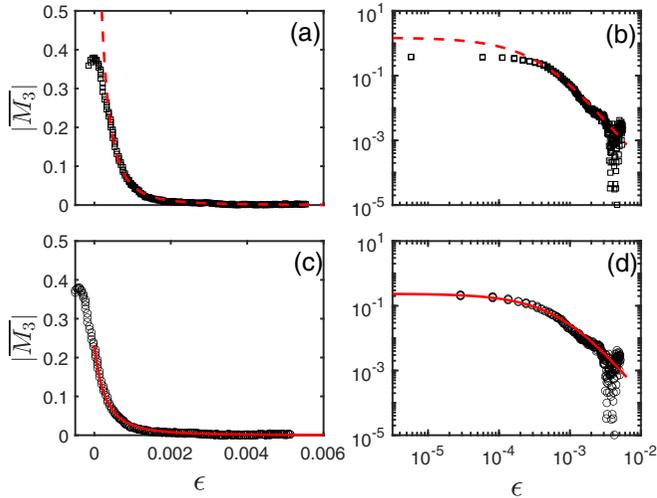
FIG. 4. Comparison between the measured third-harmonic response $|\overline{M_3}|$ (circle and square black symbols, in arbitrary units) for Pb and the theoretical results obtained from Eq. (17) (dashed and solid red lines). Data shown in (a, c) linear and (b, d) logarithmic scales. Fit parameters are shown in Table I. In (a) and (b), the fit parameter is the critical field $\tilde{H}_{c2}$ in Table I, whereas the critical temperature is set to its experimental value $T_c^{(expt)}$. In (c) and (d), the fit parameters are H_{c2} and T_c. The anisotropy parameter is set to $r = 10$.

FIG. 5. Comparison between the measured third-harmonic response $|\overline{M_3}|$ (circle and square blue symbols, in arbitrary units) for Nb and the theoretical results obtained from Eq. (17) (dashed and solid red lines). Data shown in (a, c) linear and (b, d) logarithmic scales. Fit parameters are shown in Table I. In (a) and (b), the fit parameter is the critical field $\tilde{H}_{c2}$ in Table I, whereas the critical temperature is set to its experimental value $T_c^{(expt)}$. In (c) and (d), the fitting parameters are H_{c2} and T_c. The anisotropy parameter is set to $r = 10$.

coil, but the true value could be modified by demagnetization factors (especially very close and below T_c) by up to a factor of ~ 2. Hereafter, for concreteness, we will use $H_0 = 1.3$ Oe for all cases. Since these materials are rather three dimensional, we expect the z-axis correlation length ξ_z to be larger than the layer distance s in the LD model, i.e., $r > 4$. Thus, because the reduced temperatures probed are very small ($\epsilon_{max} \sim 10^{-2}$), the precise value of r does not significantly affect the temperature dependence of $|\overline{M_3}|$ in the experimentally relevant temperature regime [as shown in Fig. 3(b)]. Therefore, to minimize the number of fitting parameters, we set $r = 10$ in all cases. This leaves only two free parameters, H_{c2} and T_c.

The comparison between theoretical and experimental results is shown Figs. 4, 5, and 6 for Pb, Nb, and V, respectively.

TABLE I. Experimental critical temperature and critical field values, $T_c^{(expt)}$ and $H_{c2}^{(expt)}$, compared to the theoretical fitting parameters T_c, $\tilde{H}_{c2}$, and H_{c2}. $\tilde{H}_{c2}$ corresponds to the fits in Figs. 4(a), 4(b), 5(a), 5(b), 6(a), and 6(b), where T_c is forced to be equal to the temperature where the experimental third-harmonic response displays a maximum (denoted here by $T_c^{(expt)}$). On the other hand, H_{c2} corresponds to the fits in Figs. 4(c), 4(d), 5(c), 5(d), 6(c), and 6(d), where T_c is allowed to be different from the experimental value. The $H_{c2}^{(expt)}$ values for Nb and V are the smallest ones reported in Ref. [55], whereas $H_{c2}^{(expt)}$ for Pb was estimated as explained in the text.

	$T_c^{(expt)}$(K)	$H_{c2}^{(expt)}$(G)	$\tilde{H}_{c2}$ (G)	H_{c2} (G)	$T_c^{(expt)}/T_c$
Pb	7.18	273	2170	1083	0.9996
Nb	9.31	1710	166	371	0.9955
V	5.29	1200	1300	520	0.9980

In all figures, the circle and square symbols correspond to data, whereas dashed and solid lines correspond to theoretical results. Experimental measurements of $|\overline{M_3}|$ become challenging below $\epsilon \sim 10^{-4}$ due to thermometry resolution
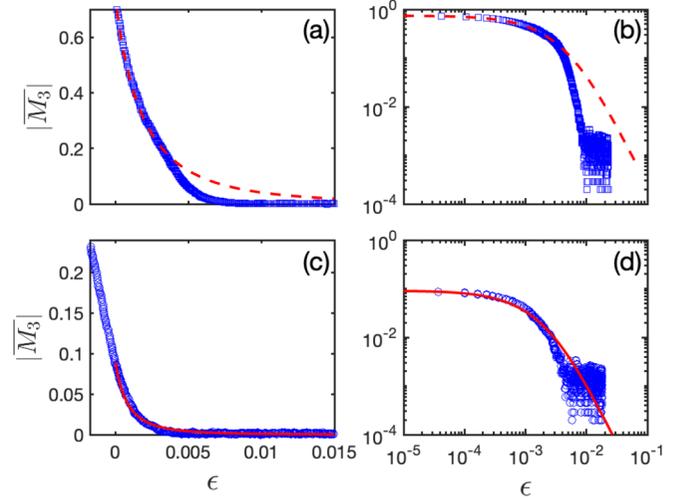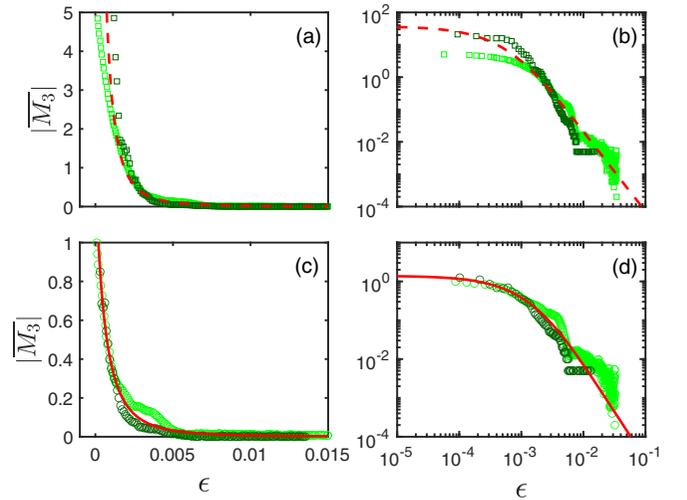

FIG. 6. Comparison between the measured third-harmonic response $|\overline{M_3}|$ (circle and square green symbols, in arbitrary units) for V and the theoretical results obtained from Eq. (17) (dashed and solid red lines). Data from two different samples are presented (light green and dark green symbols). Data shown in (a, c) linear and (b, d) logarithmic scales. Fit parameters are shown in Table I. In (a) and (b), the fit parameter is the critical field $\tilde{H}_{c2}$ in Table I, whereas the critical temperature is set to its experimental value $T_c^{(expt)}$. In (c) and (d), the fit parameters are H_{c2} and T_c. The anisotropy parameter is set to $r = 10$.

issues, and the signal typically decays below the noise level around $\epsilon \sim 10^{-2}$, indicating a small temperature regime of significant superconducting fluctuations. In the case of V, a kink is observed in one sample (light green symbols), which is possibly a spurious signal due to solder superconductivity or the result of a slight macroscopic sample inhomogeneity. For this reason, we also include results from a second sample (dark green symbols). Because the overall magnitude of the experimental $|\overline{M}_3|$ is arbitrary and changes with modifications of the setup, we rescaled the $|\overline{M}_3|$ values of the second sample (dark green symbols) by an overall constant to better match the behavior of $|\overline{M}_3|$ of the first sample (light green symbols) at larger ϵ values.

In order to obtain the best fit, we considered two slightly different procedures. In Figs. 4(a), 4(b), 5(a), 5(b), 6(a), and 6(b) (dashed lines), we fixed T_c to be the temperature at which the third-harmonic response displays a maximum; we refer to this value as $T_c^{(\mathrm{expt})}$. It is important to note, however, that this value is not necessarily the exact temperature of zero resistance onset. For this reason, and given the intrinsic experimental uncertainties in the precise absolute determination of T_c, in Figs. 4(c), 4(d), 5(c), 5(d), 6(c), and 6(d) (solid lines) we allowed T_c to vary from $T_c^{(\mathrm{expt})}$, but by no more than 0.5%. The fit parameters are shown in Table I, together with the experimental values for $T_c^{(\mathrm{expt})}$ and $H_{c2}^{(\mathrm{expt})}$, the latter taken from Ref. [55]. Note that, to distinguish between the two fitting procedures, we denote by $\tilde{H}_{c2}$ the value used in Figs. 4(a), 4(b), 5(a), 5(b), 6(a), and 6(b). Moreover, since Pb is a type-I superconductor, $H_{c2}^{(\mathrm{expt})}$ was estimated through $\sqrt{2}\kappa H_c$ [56], with $\kappa = 0.24$ [57,58] and $H_c = 803$ Oe [57,59].

Figures 4(a), 4(b), 5(a), 5(b), 6(a), and 6(b) show that the theoretical curves obtained by fixing $T_c = T_c^{(\mathrm{expt})}$ provide a reasonable description of the third-harmonic data in the region not too close to T_c for Pb and V (Figs. 4 and 6), and in the region close to T_c for Nb (Fig. 5). In particular, the latter does not seem to display the characteristic $\epsilon^{-5/2}$ power-law behavior observed in the former two in the regime of intermediate ϵ values. However, because of the definition of the reduced temperature, $\epsilon = \frac{T - T_c}{T_c}$, even small changes in T_c within typical experimental uncertainty could account for these deviations between theory and experiment. As noted above, to address this issue we performed a second fit procedure allowing T_c to be slightly different than $T_c^{(\mathrm{expt})}$. As shown in Figs. 4(c), 4(d), 5(c), 5(d), 6(c), and 6(d), we find a better agreement between the theoretical and experimental results over a wider temperature range, including in the case of Nb in the intermediate ϵ range. Comparing the theoretical T_c values in Table I with the $T_c^{(\mathrm{expt})}$ values, we note that in all cases T_c is slightly larger than $T_c^{(\mathrm{expt})}$. This is the reason why in Figs. 4(c), 4(d), 5(c), 5(d), 6(c), and 6(d) the theoretical curves stop at $\epsilon = 0$ whereas the data extend to the region $\epsilon < 0$.

On the other hand, there is a more significant difference between H_{c2} and the experimental value $H_{c2}^{(\mathrm{expt})}$ taken from the literature, with the former being a factor of approximately 2 to 6 smaller or larger than the latter. We note that the intrinsic uncertainty in the precise value of H_0 in our experiment may explain at least part of this discrepancy. Moreover, the value of $H_{c2}^{(\mathrm{expt})}$ strongly depends on material preparation details, especially for polycrystalline samples where significant internal
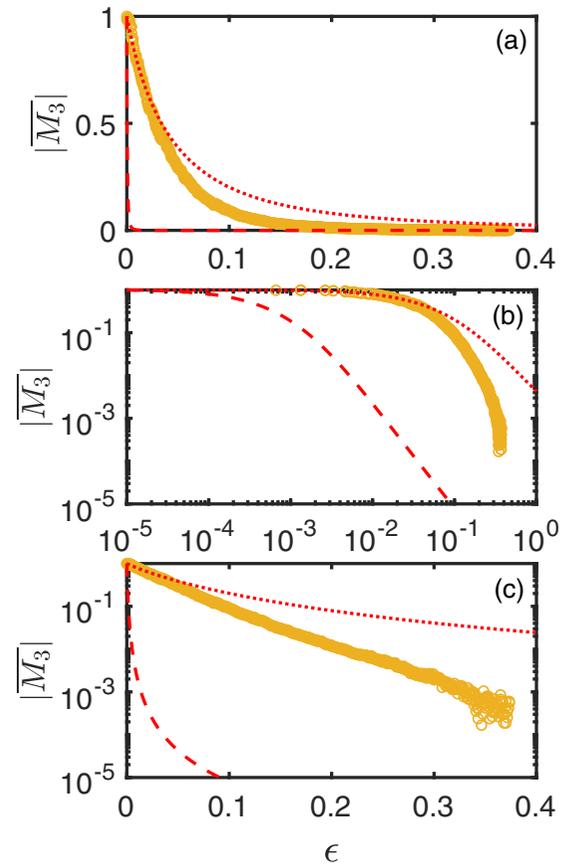

FIG. 7. Comparison between the experimentally measured third-harmonic response $|\overline{M}_3|$ (orange symbols, in arbitrary units) for SRO and the theoretical results obtained from Eq. (17) (dashed and dotted red lines). Data shown in (a) linear, (b) logarithmic, and (c) semilog-arithmic scales. For the theoretical curves, the critical temperature is set to its experimental value $T_c^{(\mathrm{expt})}$ whereas the critical field is set to $H_{c2}^{(\mathrm{expt})}$ (dashed lines) and to $0.01 H_{c2}^{(\mathrm{expt})}$ (dotted lines). The anisotropy parameter is set to $r = 10$.

strains can be present [60]. In principle, the critical fields are lower in more pristine materials, and it is therefore meaningful to take the lowest known experimental values (taken from Ref. [55]) for our comparison. Finally, while the LD model employed here to calculate $|\overline{M}_3|$ assumes a layered system, the bulk elemental superconductors are cubic. On top of that, the LD approach of including only Gaussian fluctuations is expected to break down below a very small ϵ_{crit}, whose precise value is likely different for distinct materials. Despite these drawbacks, this comparison shows that the LD model for the third-harmonic response $|\overline{M}_3|$ due to contributions from superconducting fluctuations provides a satisfactory description of the experimental results.

B. Strontium ruthenate (Sr_2RuO_4)

Having validated our theoretical approach to compute the third-harmonic response $|\overline{M}_3|$ by comparison with data for elemental superconductors, we now perform the same comparison with the lamellar perovskite-derived superconductor Sr_2RuO_4 (SRO). The main advantage of our LD calculation of $|\overline{M}_3|$ is that it is entirely phenomenological and
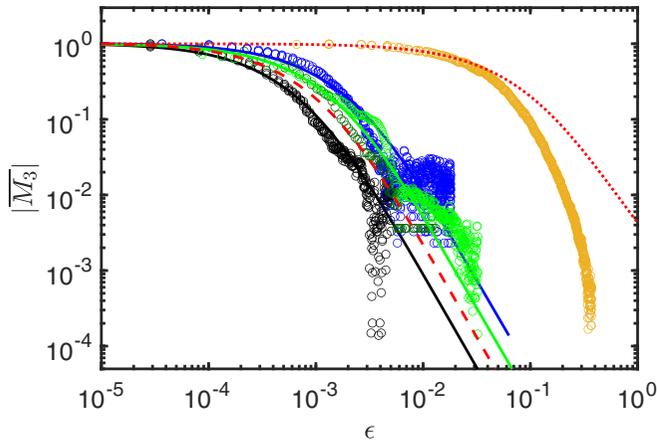
FIG. 8. Comparison between the normalized third-harmonic response data and the theoretical $|\overline{M}_3|$ results for Pb, Nb, V, and SRO on a logarithmic scale. The solid lines correspond to the best fits in Figs. 4, 5, and 6, which refer to the conventional superconductors, whereas the dashed and dotted lines correspond to the fits for SRO in Fig. 7.

independent of microscopic details. In fact, the main assumption is that the superconducting fluctuations can be described by a Gaussian approximation. Consequently, the calculation could in principle be applicable to unconventional superconductors as well.

SRO is believed to host an unconventional superconducting state that breaks time-reversal symmetry [61–63]. Whereas for a long time SRO was considered a promising candidate for *p*-wave triplet superconductivity [64,65], recent experiments have revealed problems with this interpretation [66–68]. This has motivated alternative proposals involving, e.g., *d*-wave and *g*-wave superconductivity [69–74]. As mentioned above, the data presented here are the same as in Ref. [4]. As shown there, the third-harmonic response of other perovskite-based superconductors like strontium titanate and the cuprates display a similar unusual temperature dependence.

The data for SRO are shown by the orange symbols in Fig. 7 on linear scale [Fig. 7(a)], logarithmic scale [Fig. 7(b)], and semilogarithmic scale [Fig. 7(c)]. The theoretical results for $|\overline{M}_3|$ are plotted in the same panels using the experimental critical temperature value, $T_c = 1.51$ K $= T_c^{(\text{expt})}$, and two different critical field values: $H_{c2} = 750$ G $= H_{c2}^{(\text{expt})}$ (dashed lines) and $H_{c2} = 7.6$ G $\approx 0.01 H_{c2}^{(\text{expt})}$ (dotted lines). Here, $T_c^{(\text{expt})}$ corresponds to the temperature at which the third-harmonic response is maximum, and $H_{c2}^{(\text{expt})}$ is the experimental value reported in the literature [64,75]. The key observation is that the theoretical $|\overline{M}_3|$ curve with $H_{c2} = H_{c2}^{(\text{expt})}$ grossly underestimates the data. It is necessary to reduce H_{c2} by two orders of magnitude to obtain values that are comparable between theory and experiment. In contrast, for the elemental superconductors, the difference in the theoretical and experimental H_{c2} values was at most a factor of 6. More importantly, even by changing H_{c2} by such a large amount, the temperature dependence of the data is not captured by the theoretical $|\overline{M}_3|$ curve, in contrast again to the case of conventional superconductors. Indeed, while the theo-
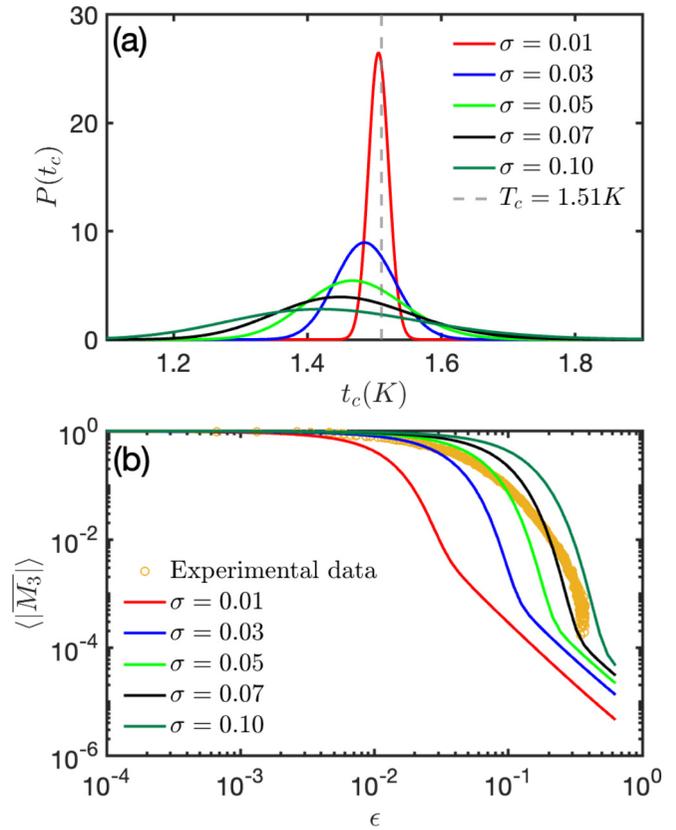

FIG. 9. (a) Normalized probability distribution function of the critical temperature t_c for different values of the parameter σ in Eq. (20). Here, the parameter μ is fixed by the condition $v_F(T_c^{(\text{expt})}) = 0.3$, with $T_c^{(\text{expt})} = 1.51$ K (indicated by the dashed gray vertical line) and the temperature-dependent superconducting volume fraction v_F defined by Eq. (22). (b) Averaged third-harmonic response $\langle |\overline{M}_3| \rangle$ calculated from the distribution functions of (a), compared to the data for SRO, as a function of $\epsilon = \frac{T}{T_c} - 1$. In this calculation, we used the experimental values $T_c^{(\text{expt})} = 1.51$ K and $H_{c2}^{(\text{expt})} = 750$ G, and set $r = 10$.

retical $|\overline{M}_3|$ curve shows a power-law for intermediate reduced temperatures, the data display an accurately exponential temperature dependence, as discussed in Ref. [4] and shown in Fig. 7(c). We note that the experimental H_{c2} value depends very strongly on the orientation of the field with respect to the crystalline *c* axis, such that a small misalignment can lead to sizable variation [75]. However, the discrepancy between the theoretical and experimental results cannot be explained by sample misalignment, since the critical field *increases* with increasing angle between the field direction and the crystalline *c* axis, whereas our theoretical results require *smaller* H_{c2} values.

Figure 8 summarizes the third-harmonic response $|\overline{M}_3|$ of the three conventional superconductors studied here (Pb, Nb, and V), as well as of the unconventional superconductor SRO. The differences between SRO and the conventional superconductors are not only on the temperature dependence of $|\overline{M}_3|$, but also on the fact that $|\overline{M}_3|$ is larger and extends over a much wider relative temperature range in SRO. Indeed, while superconducting fluctuations are detected up to $\epsilon \sim 10^{-2}$ in

conventional superconductors, they extend all the way up to $\epsilon \sim 1$ in SRO.

To attempt to address the discrepancy between the theoretical and experimental results for SRO, we revisit the assumptions behind the LD model, from which we derived the expression for $|\overline{M_3}|$. As discussed above, the LD model makes no reference to the microscopic pairing mechanism. However, it does assume a homogeneous system. In contrast, perovskites are known for their intrinsic inhomogeneity, arising from, e.g., oxygen vacancies and local structural distortions that deviate strongly from the average lattice structure (see Ref. [50] and references therein). Indeed, the experiments of Ref. [4] indicate that universal structural inhomogeneity is present in perovskite-based superconductors such as SRO. It has also been argued that dislocations can have a strong impact on the superconducting state properties of several perovskites [74,76,77]. In the particular case of SRO, muon spin-rotation measurements find a rather inhomogeneous signature of time-reversal-symmetry breaking below T_c [63]. It is also known that the T_c of SRO is strongly dependent on stress [63,78], implying that inhomogeneous internal stresses would lead to regions with locally modified T_c. Simple point disorder also leads to a variation of the local critical temperature [79]. Indeed, scanning SQUID measurements have directly detected T_c inhomogeneity on the micron scale [80].

The impact of inhomogeneity on superconducting properties has been studied by a variety of approaches [15,51,81–83]. Here, we consider a phenomenological approach that introduces a probability distribution of the local T_c (see also Ref. [84]). Such an inhomogeneous T_c distribution may explain why the superconducting fluctuations in SRO are stronger and extend to higher reduced temperatures as compared to conventional superconductors, since regions with a locally higher T_c are expected to result in a much larger contribution to $|\overline{M_3}|$ than that arising from the rest of the sample. To test this idea, we include a distribution function for T_c into our LD-based phenomenological model. We denote the "transition temperature variable" as t_c, and reserve the notation T_c for the actual transition temperature of the system to avoid confusion. The form of the distribution function $P(t_c)$ depends on several sources of inhomogeneity in the system (see, for instance, Ref. [51]). A microscopic derivation is thus very challenging, and beyond the scope of this work. Instead, here we opt for a simple phenomenological modeling of $P(t_c)$. In particular, we employ a normalized log-normal distribution:

$$P(t_c) = \frac{1}{t_c \sqrt{2\pi\sigma^2}} \exp\left[-\frac{\left(\ln \frac{t_c}{\mu}\right)^2}{2\sigma^2}\right], \quad (20)$$

where μ and σ are positive parameters that determine the mean value and variance of the distribution. The choice of

this distribution is motivated by its properties of only allowing nonzero values of t_c and of having long tails toward larger values of t_c. We note that a log-normal distribution for the local gap—and consequently of the local T_c—was previously derived theoretically in Ref. [84] for disordered quasi-two-dimensional superconductors in the limit of weak multifractality, and observed experimentally in weakly disordered monolayer $NbSe_2$ [85]. The averaged fluctuation magnetization in Eq. (4) acquires the following form:

$$\langle M \rangle(\epsilon) = \int_0^T \frac{dt_c}{t_c \sqrt{2\pi\sigma^2}} \exp\left[-\frac{\left(\ln \frac{t_c}{\mu}\right)^2}{2\sigma^2}\right] M\left(\frac{T}{t_c} - 1\right) \quad (21)$$

with $M(\epsilon)$ given by Eq. (4). We can then compute the averaged third-harmonic response $\langle|\overline{M_3}|\rangle$ from Eq. (17). We assume that $\langle|\overline{M_3}|\rangle$ is dominated by superconducting fluctuation contributions, which appear only in regions that are locally nonsuperconducting (i.e., for which $\epsilon = \frac{T}{t_c} - 1$ is positive). For this reason, the limits of the t_c integration are such that $0 < t_c < T$.

The two parameters characterizing the distribution function, μ and σ, are not independent, since they are related by the value of T_c. To see that, we first define the temperature-dependent superconducting volume fraction $v_F(T)$, which is given by

$$v_F(T) = 1 - \int_0^T P(t_c)dt_c = \frac{1}{2} - \frac{1}{2}\text{erf}\left(\frac{\ln \frac{t_c}{\mu}}{\sqrt{2}\sigma}\right), \quad (22)$$

since the integral on the right-hand side gives the nonsuperconducting volume fraction ($T > t_c$). When the volume fraction becomes larger than a threshold value v_F^*, the local superconducting regions are expected to percolate and the whole sample becomes superconducting. Note that a similar criterion was used in the analysis of Ref. [84]. T_c is then obtained by solving the equation $v_F(T_c) = v_F^*$,

$$\frac{\mu}{T_c} = \exp[-\sqrt{2}\sigma\,\text{erf}^{-1}(1 - 2v_F^*)], \quad (23)$$

where $\text{erf}^{-1}(x)$ is the inverse error function. For simplicity, we use for v_F^* the site percolation threshold value for a cubic lattice, $v_F^* = 0.3$. While v_F^* itself could be considered a free parameter, we opt to fix it to avoid increasing the number of fitting parameters. As a result, the only additional parameter needed to compute $\langle|\overline{M_3}|\rangle$, as compared to the "clean" system $|\overline{M_3}|$, is the dimensionless σ, which determines the width of the distribution. In Fig. 9(a), we illustrate the profile of $P(t_c)$ for different values of σ under the constraint $v_F(T_c^{(\text{expt})}) = 0.3$. The full expression for $\langle|\overline{M_3}|\rangle$ then becomes

$$\frac{\langle|\overline{M_3}|\rangle(\epsilon)}{M_\infty} = \frac{24(\epsilon+1)}{\pi \ln 2} \int_0^1 \frac{dx}{x\sqrt{2\pi\sigma^2}} \exp\left\{-\left[\frac{\ln(x\epsilon+x)}{\sqrt{2}\sigma} + \text{erf}^{-1}(1 - 2v_F^*)\right]^2\right\} \int_{-\pi/2}^{\pi/2} \mathcal{M}(x, h_0\cos\theta)\cos 3\theta\, d\theta \quad (24)$$

with

$$\mathcal{M}(x, h) = -\int_0^{\frac{\pi}{2}} d\phi \left\{\frac{\frac{1}{x} - 1 + r\sin^2\phi}{2h}\left[\psi\left(\frac{\frac{1}{x} - 1 + r\sin^2\phi}{2h} + \frac{1}{2}\right) - 1\right] - \ln\Gamma\left(\frac{\frac{1}{x} - 1 + r\sin^2\phi}{2h} + \frac{1}{2}\right) + \frac{1}{2}\ln(2\pi)\right\}. \tag{25}$$
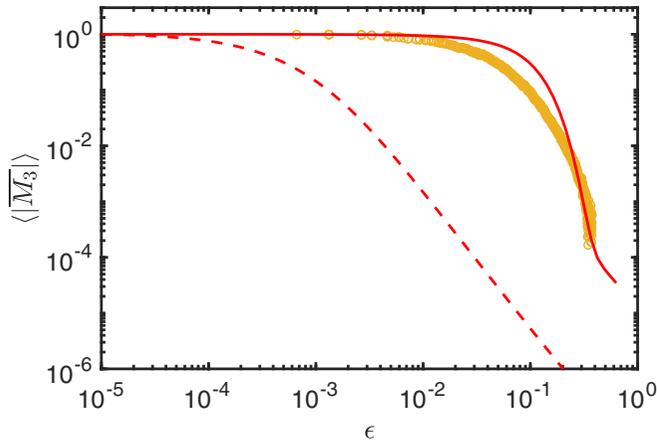
FIG. 10. Averaged third-harmonic response $\langle|\overline{M}_3|\rangle$ as a function of the reduced temperature $\epsilon = \frac{T}{T_c} - 1$ calculated using the parameters $T_c = 1.41$ K $\approx 0.93 T_c^{(\text{expt})}$ and $\sigma = 0.08$, while keeping $H_{c2} = H_{c2}^{(\text{expt})} = 750$ G and $r = 10$ (solid red line). The orange symbols are the experimental results, and the dashed red line reproduces the theoretical third-harmonic response $|\overline{M}_3|$ of the clean system with $T_c = T_c^{(\text{expt})}$ and $H_{c2} = H_{c2}^{(\text{expt})}$.

Using the distribution functions of Fig. 9(a), in Fig. 9(b) we present the calculated averaged third-harmonic response $\langle|\overline{M}_3|\rangle$ (solid red line) using the experimentally determined values for T_c and H_{c2}. The comparison with the data shows that even a relatively mild width of the distribution of t_c values, with $\sigma \lesssim 0.1$, is capable of capturing the extended temperature window for which the third-harmonic response is sizable. As anticipated, this behavior is a consequence of the fact that regions with a local higher T_c value, although occupying a small volume, provide a sizable contribution to the third-harmonic response.

The temperature dependence of the third-harmonic response data, however, is not very well captured by the theoretical curves in Fig. 9(b). To try to address this issue, we promote T_c to a free parameter and allow it to deviate slightly from the experimental value $T_c^{(\text{expt})} = 1.51$ K. Figure 10 shows the results for $\langle|\overline{M}_3|\rangle$ in the case of $T_c = 1.41$ K $\approx 0.93 T_c^{(\text{expt})}$ and $\sigma = 0.08$. Clearly, the temperature dependence of the calculated $\langle|\overline{M}_3|\rangle$ becomes more similar to the experimentally measured one, but still fails to capture it completely. Thus, our conclusion is that while T_c inhomogeneity may explain the extended temperature range where the third-harmonic response is sizable, it is unlikely to explain the exponential tail of $|\overline{M}_3|$ observed experimentally in Ref. [4].

IV. CONCLUDING REMARKS

In this work, we used the LD model to compute the third-harmonic magnetic response $|\overline{M}_3|$ due to Gaussian superconducting fluctuations. Due to its phenomenological nature, the LD model could in principle be applicable to both conventional and unconventional superconductors. Our detailed comparison with measurements of $|\overline{M}_3|$ found that the theoretical modeling provides a good description of the

data in the case of Pb, Nb, and V—provided that the critical field is properly modified from its experimental value—but a rather poor account of the data for SRO. Inclusion of T_c inhomogeneity, which is intrinsically present in SRO, improved significantly the agreement between theoretical model and experimental data, although the model could not properly capture the experimentally observed exponential temperature dependence of $|\overline{M}_3|$ (see Ref. [4]).

Further investigation is thus required to elucidate the origin of this exponential behavior of $|\overline{M}_3|$, which was also seen in other perovskite superconductors such as SrTiO$_3$ (STO) and the cuprates, and appears to be quite robust [4]. One cannot completely discard simple T_c inhomogeneity as the source of this effect, since here we only focused on a very specific and particularly simple distribution function for T_c. While this choice allowed us to argue on a more quantitative basis that T_c inhomogeneity can explain why $|\overline{M}_3|$ remains large over a wide temperature window in SRO, the actual T_c distribution is certainly more complicated and likely material dependent. A phenomenological T_c distribution will likely require fine tuning to give an exponential temperature dependence of the third-harmonic response. Nevertheless, if rare regions are present, they might give rise to specific tails in the distribution function that may be common to different materials; these types of effects have been explored in more detail in Refs. [50,51]. We also note that, in the particular case of the cuprates, an exponential temperature-dependent behavior associated with superconducting fluctuations was also observed in other observables such as linear and nonlinear conductivity and specific heat, and described in terms of a Gaussian T_c distribution [14,15]. It would be interesting to investigate whether the exponential temperature dependence observed in the third-harmonic response of SRO is also manifested in these other observables in the case of SRO. In fact, as shown in Ref. [4], prior specific heat data [86] are consistent with this possibility.

Different effects could be the root of the remaining discrepancy between the SRO data and the model with inhomogeneities. One effect specific to SRO is that, if this system is indeed a time-reversal symmetry-breaking (TRSB) two-component superconductor, as proposed by different models [71–74], the superconducting fluctuation spectrum will likely be more complicated than that of the LD model. However, the fact that the same exponential temperature dependence of $|\overline{M}_3|$ is seen in STO and cuprates, the latter being single-component superconductors, renders this scenario less likely. Moreover, TRSB likely manifests itself primarily in the second-harmonic response, and only below T_c. Another potential reason for the discrepancy is the central approximation of the LD model of solely Gaussian superconducting fluctuations. This raises the interesting question whether non-Gaussian fluctuations, such as those associated with the long tail in the distribution of T_c of disordered superconductors discussed in Ref. [51], might also play an important role in the fluctuation spectra of perovskite superconductors.

[1] A. A. Varlamov, A. Galda, and A. Glatz, Rev. Mod. Phys. **90**, 015009 (2018).

[2] A. Larkin and A. Varlamov, *Theory of Fluctuations in Superconductors* (Clarendon Press, Oxford, 2005).

[3] A. Buzdin and V. Dorin, in *Fluctuation Phenomena in High Temperature Superconductors* (Springer, Berlin, 1997), pp. 335–341.

[4] D. Pelc, Z. Anderson, B. Yu, C. Leighton, and M. Greven, Nat. Commun. **10**, 2729 (2019).

[5] T. Suzuki and T. Tsuboi, J. Phys. Soc. Jpn. **43**, 444 (1977).

[6] T. Tsuboi and T. Suzuki, J. Phys. Soc. Jpn. **42**, 437 (1977).

[7] J. L. Tallon, J. G. Storey, and J. W. Loram, Phys. Rev. B **83**, 092502 (2011).

[8] R. Glover, Phys. Lett. A **25**, 542 (1967).

[9] M. Strongin, O. F. Kammerer, J. Crow, R. S. Thompson, and H. L. Fine, Phys. Rev. Lett. **20**, 922 (1968).

[10] S. T. Ruggiero, T. W. Barbee, and M. R. Beasley, Phys. Rev. Lett. **45**, 1299 (1980).

[11] D. I. Mircea, H. Xu, and S. M. Anlage, Phys. Rev. B **80**, 144505 (2009).

[12] F. Rullier-Albenque, H. Alloul, and G. Rikken, Phys. Rev. B **84**, 014522 (2011).

[13] C. Carbillet, S. Caprara, M. Grilli, C. Brun, T. Cren, F. Debontridder, B. Vignolle, W. Tabis, D. Demaille, L. Largeau *et al.*, Phys. Rev. B **93**, 144509 (2016).

[14] P. Popčević, D. Pelc, Y. Tang, K. Velebit, Z. W. Anderson, V. Nagarajan, G. Yu, M. Požek, N. Barišić, and M. Greven, npj Quantum Mater. **3**, 42 (2018).

[15] D. Pelc, M. Vučković, M. S. Grbić, M. Požek, G. Yu, T. Sasagawa, M. Greven, and N. Barišić, Nat. Commun. **9**, 4327 (2018).

[16] R. Corson, L. Mallozzi, J. Orenstein, J. N. Eckstein, and Božović, Nature (London) **398**, 221 (1999).

[17] J. Orenstein, J. Corson, S. Oh, and J. N. Eckstein, Ann. Phys. **15**, 596 (2006).

[18] M. S. Grbić, M. Požek, D. Paar, V. Hinkov, M. Raichle, D. Haug, B. Keimer, N. Barišić, and A. Dulčić, Phys. Rev. B **83**, 144508 (2011).

[19] L. S. Bilbro, L. Valdes Aguilar, G. Logvenov, O. Pelleg, I. Božović, and N. P. Armitage, Nat. Phys. **7**, 298 (2011).

[20] T. H. Geballe, A. Menth, F. J. Di Salvo, and F. R. Gamble, Phys. Rev. Lett. **27**, 314 (1971).

[21] J. P. Gollub, M. R. Beasley, R. Callarotti, and M. Tinkham, Phys. Rev. B **7**, 3039 (1973).

[22] L. Li, Y. Wang, S. Komiya, S. Ono, Y. Ando, G. D. Gu, and N. P. Ong, Phys. Rev. B **81**, 054510 (2010).

[23] I. Kokanović, D. J. Hills, M. L. Sutherland, R. Liang, and J. R. Cooper, Phys. Rev. B **88**, 060505(R) (2013).

[24] S. Kasahara, T. Yamashita, A. Shi, R. Kobayashi, Y. Shimoyama, T. Watashige, K. Ishida, T. Terashima, T. Wolf, F. Hardy *et al.*, Nat. Commun. **7**, 12843 (2016).

[25] G. Yu, D.-D. Xia, D. Pelc, R.-H. He, N.-H. Kaneko, T. Sasagawa, Y. Li, X. Zhao, N. Barišić, A. Shekhter, A. Shekhter, and M. Greven, Phys. Rev. B **99**, 214502 (2019).

[26] Y. Wang, L. Li, and N. P. Ong, Phys. Rev. B **73**, 024510 (2006).

[27] F. Rullier-Albenque, R. Tourbot, H. Alloul, P. Lejay, D. Colson, and A. Forget, Phys. Rev. Lett. **96**, 067002 (2006).

[28] J. Chang, N. Doiron-Leyraud, O. Cyr-Choiniere, G. Grissonnanche, F. Laliberté, E. Hassinger, J.-P. Reid, R. Daou, S. Pyon, T. Takayama *et al.*, Nat. Phys. **8**, 751 (2012).

[29] F. F. Tafti, F. Laliberté, M. Dion, J. Gaudet, P. Fournier, and L. Taillefer, Phys. Rev. B **90**, 024519 (2014).

[30] K. Behnia and H. Aubin, Rep. Prog. Phys. **79**, 046502 (2016).

[31] H. Schmidt, Z. Phys. A **216**, 336 (1968).

[32] V. V. Shmidt, JETP **27**, 142 (1968).

[33] K. Maki, Prog. Theor. Phys. **39**, 897 (1968).

[34] R. S. Thompson, Phys. Rev. B **1**, 327 (1970).

[35] A. Schmid, Phys. Rev. **180**, 527 (1969).

[36] R. E. Prange, Phys. Rev. B **1**, 2349 (1970).

[37] E. Abrahams, M. Redi, and J. W. F. Woo, Phys. Rev. B **1**, 208 (1970).

[38] J. Kurkijärvi, V. Ambegaokar, and G. Eilenberger, Phys. Rev. B **5**, 868 (1972).

[39] L. G. Aslamazov and A. I. Larkin, Sov. Phys. JETP **40**, 321 (1974).

[40] V. Emery and S. Kivelson, Nature (London) **374**, 434 (1995).

[41] A. Glatz, A. A. Varlamov, and V. M. Vinokur, Phys. Rev. B **84**, 104510 (2011).

[42] S. Ullah and A. T. Dorsey, Phys. Rev. B **44**, 262 (1991).

[43] D. S. Fisher, M. P. A. Fisher, and D. A. Huse, Phys. Rev. B **43**, 130 (1991).

[44] L. B. Ioffe, A. I. Larkin, A. A. Varlamov, and L. Yu, Phys. Rev. B **47**, 8936 (1993).

[45] I. Ussishkin, S. L. Sondhi, and D. A. Huse, Phys. Rev. Lett. **89**, 287001 (2002).

[46] M. N. Serbyn, M. A. Skvortsov, A. A. Varlamov, and V. Galitski, Phys. Rev. Lett. **102**, 067001 (2009).

[47] K. Michaeli and A. M. Finkel'stein, Europhys. Lett. **86**, 27007 (2009).

[48] S. Li and A. Levchenko, Ann. Phys. **417**, 168137 (2020).

[49] W. Lawrence and S. Doniach, in *Proceedings of the 12th International Conference on Low Temperature Physics*, edited by E. Kanda (Tokyo Keigaku Publishing, Tokyo, 1971), pp. 361–362.

[50] D. Pelc, R. J. Spieker, Z. W. Anderson, M. J. Krogstad, N. Biniskos, N. G. Bielinski, B. Yu, T. Sasagawa, L. Chauviere, P. Dosanjh *et al.*, arXiv:2103.05482.

[51] J. F. Dodaro and S. A. Kivelson, Phys. Rev. B **98**, 174503 (2018).

[52] T. Mishonov and E. Penev, Int. J. Mod. Phys. B **14**, 3831 (2000).

[53] T. Tsuzuki and M. Koyanagi, Phys. Lett. A **30**, 545 (1969).

[54] D. Drobac, Z. Marohnic, I. Zivkovic, and M. Prester, Rev. Sci. Instrum. **84**, 054708 (2013).

[55] D. R. Lide, *CRC Handbook of Chemistry and Physics* (CRC Press, Boca Raton, FL, 2004), Vol. 84.

[56] M. Tinkham, *Introduction to Superconductivity* (Courier Corporation, New York, 2004).

[57] F. W. Smith, Ph.D. thesis, Brown University, 1969.

[58] D. E. Farrell, B. S. Chandrasekhar, and H. V. Culbert, Phys. Rev. **177**, 694 (1969).

[59] W. Martienssen and H. Warlimont, *Springer Handbook of Condensed Matter and Materials Data* (Springer, Berlin, 2005).

[60] G. J. Van Gurp, Philips Res. Rep. **22**, 10 (1967).

[61] G. M. Luke, Y. Fudamoto, K. Kojima, M. Larkin, J. Merrin, B. Nachumi, Y. Uemura, Y. Maeno, Z. Mao, Y. Mori *et al.*, Nature (London) **394**, 558 (1998).

[62] J. Xia, Y. Maeno, P. T. Beyersdorf, M. M. Fejer, and A. Kapitulnik, Phys. Rev. Lett. **97**, 167002 (2006).

[63] V. Grinenko, S. Ghosh, R. Sarkar, J.-C. Orain, A. Nikitin, M. Elender, D. Das, Z. Guguchia, F. Brückner, M. E. Barber *et al.*, Nat. Phys. **21**, 748 (2021).

[64] A. P. Mackenzie and Y. Maeno, Rev. Mod. Phys. **75**, 657 (2003).

[65] C. Kallin, Rep. Prog. Phys. **75**, 042501 (2012).

[66] A. P. Mackenzie, T. Scaffidi, C. W. Hicks, and Y. Maeno, npj Quantum Mater. **2**, 40 (2017).

[67] A. Pustogow, Y. Luo, A. Chronister, Y.-S. Su, D. Sokolov, F. Jerzembeck, A. P. Mackenzie, C. W. Hicks, N. Kikugawa, S. Raghu *et al.*, Nature (London) **574**, 72 (2019).

[68] A. Chronister, A. Pustogow, N. Kikugawa, D. A. Sokolov, F. Jerzembeck, C. W. Hicks, A. P. Mackenzie, E. D. Bauer, and S. E. Brown, Proc. Natl. Acad. Sci. USA **118**, e2025313118 (2021).

[69] H. S. Røising, T. Scaffidi, F. Flicker, G. F. Lange, and S. H. Simon, Phys. Rev. Research **1**, 033108 (2019).

[70] A. Ramires and M. Sigrist, Phys. Rev. B **100**, 104501 (2019).

[71] A. T. Rømer, D. D. Scherer, I. M. Eremin, P. J. Hirschfeld, and B. M. Andersen, Phys. Rev. Lett. **123**, 247001 (2019).

[72] H. G. Suh, H. Menke, P. M. R. Brydon, C. Timm, A. Ramires, and D. F. Agterberg, Phys. Rev. Research **2**, 032023(R) (2020).

[73] S. A. Kivelson, A. C. Yuan, B. Ramshaw, and R. Thomale, npj Quantum Mater. **5**, 43 (2020).

[74] R. Willa, M. Hecker, R. M. Fernandes, and J. Schmalian, Phys. Rev. B **104**, 024511 (2021).

[75] S. Kittaka, T. Nakamura, Y. Aono, S. Yonezawa, K. Ishida, and Y. Maeno, Phys. Rev. B **80**, 174514 (2009).

[76] Y. Ying, N. Staley, Y. Xin, K. Sun, X. Cai, D. Fobes, T. Liu, Z. Mao, and Y. Liu, Nat. Commun. **4**, 2596 (2013).

[77] S. Hameed, D. Pelc, Z. W. Anderson, A. Klein, R. J. Spieker, L. Yue, B. Das, J. Ramberger, M. Lukas, Y. Liu, M. J. Krogstad, R. Osborn, Y. Li, C. Leighton, R. M. Fernandes, and M. Greven, arXiv:2005.00514 [Nat. Mater. (to be published)].

[78] A. Steppke, L. Zaho, M. E. Barber, T. Scaffidi, F. Jerzembeck, H. Rosner, A. S. Gibbs, Y. Maeno, S. H. Simon, A. P. Mackenzie *et al.*, Science **355**, eaaf9398 (2017).

[79] A. P. Mackenzie, R. K. W. Haselwimmer, A. W. Tyler, G. G. Lonzarich, Y. Mori, S. Nishizaki, and Y. Maeno, Phys. Rev. Lett. **80**, 161 (1998).

[80] C. A. Watson, A. S. Gibbs, A. P. Mackenzie, C. W. Hicks, and K. A. Moler, Phys. Rev. B **98**, 094521 (2018).

[81] A. Coleman, E. Yukalova, and V. Yukalov, Physica C **243**, 76 (1995).

[82] B. M. Andersen, A. Melikyan, T. S. Nunner, and P. J. Hirschfeld, Phys. Rev. B **74**, 060501(R) (2006).

[83] M. Swanson, Y. L. Loh, M. Randeria, and N. Trivedi, Phys. Rev. X **4**, 021007 (2014).

[84] J. Mayoh and A. M. García-García, Phys. Rev. B **92**, 174526 (2015).

[85] C. Rubio-Verdú, A. M. García-García, H. Ryu, D.-J. Choi, J. Zaldívar, S. Tang, B. Fan, Z.-X. Shen, S.-K. Mo, J. I. Pascual *et al.*, Nano Lett. **20**, 5111 (2020).

[86] S. Nishizaki, Y. Maeno, and Z. Mao, J. Low Temp. Phys. **117**, 1581 (1999).